NeuroImage 79 (2013) 288–294

Contents lists available at SciVerse ScienceDirect

NeuroImage

journal homepage: www.elsevier.com/locate/ynimg

Fast *in vivo* imaging of amyloid plaques using μ-MRI Gd-staining combined with ultrasound-induced blood–brain barrier opening

Mathieu D. Santin [a,b,1], Thomas Debeir [c], S. Lori Bridal [d,e], Thomas Rooney [c], Marc Dhenain [a,b,*]

[a] URA 2210 CEA/CNRS Laboratoire des maladies neurodégénératives – 18 route du Panorama-BP6 – 92265 Fontenay-aux-Roses Cedex, France
[b] CEA/I2BM/MIRCen – 18 route du Panorama-BP6 – 92265 Fontenay-aux-Roses Cedex, France
[c] Sanofi, Therapeutic Strategic Unit Aging – 1 avenue Pierre Brossolette – 91385 Chilly-Mazarin Cedex
[d] Université Pierre et Marie Curie, F-75005, Paris, France
[e] CNRS, UMR 7623, Laboratoire d'Imagerie Paramétrique, F-75006, Paris, France

ARTICLE INFO

Article history:
Accepted 25 April 2013
Available online 7 May 2013

Keywords:
Alzheimer
Amyloid
Blood–brain barrier
MRI
Ultrasound
Microbubbles

ABSTRACT

Amyloid plaques are one of the major microscopic lesions that characterize Alzheimer's disease. Current approaches to detect amyloid plaques by using magnetic resonance imaging (MRI) contrast agents require invasive procedures to penetrate the blood–brain barrier (BBB) and to deliver the contrast agent into the vicinity of amyloid plaques. Here we have developed a new protocol (US–Gd-staining) that enables the detection of amyloid plaques in the brain of an APP/PS1 transgenic mouse model of amyloidosis after intra-venous injection of a non-targeted, clinically approved MRI contrast agent (Gd-DOTA, Dotarem®) by transiently opening the BBB with unfocused ultrasound (1 MHz) and clinically approved microbubbles (Sonovue®, Bracco). This US–Gd-staining protocol can detect amyloid plaques with a short imaging time (32 min) and high in-plane resolution (29 μm). The sensitivity and resolution obtained is at least equal to that provided by MRI protocols using intra-cerebro-ventricular injection of contrast agents, a reference method used to penetrate the BBB. To our knowledge this is the first study to demonstrate the ability of MR imaging to detect amyloid plaques by using a peripheral intra-venous injection of a clinically approved NMR contrast agent.

Introduction

Alzheimer's disease (AD) is the most common neurodegenerative disease of the central nervous system and is characterized by two major microscopic lesions: amyloid plaque deposits and neurofibrillary tangles. Amyloid plaques are one of the earliest hallmarks of the disease, which can occur up to twenty years before the first clinical signs of dementia (Sperling et al., 2011) and are thought to precede and trigger a series of pathological events eventually leading to the onset of clinical AD (Hardy and Selkoe, 2002). Because of their very early occurrence, amyloid plaques are a major target for several disease modifying agents undergoing clinical development (Mangialasche et al., 2010).

In humans, amyloid plaques measure from 20 to 100 μm. Currently, PET imaging with radioactive ligands, such as the Pittsburgh compound B (PiB) radiolabeled with ^{11}C (Klunk et al., 2004) or the AV-45 radiolabeled with ^{18}F (Doraiswamy et al., 2012), is the major method used to measure global amyloid load in humans. PET imaging with ^{18}F AV-45 can also detect amyloid load in transgenic mouse models of AD (Poisnel et al., 2012), whereas contradictory results concerning the ability of ^{11}C PiB-PET to detect amyloid plaques in transgenic mouse models have been reported in other studies (Klunk et al., 2005; Maeda et al., 2011). Although PET has been widely used for brain imaging, it suffers from some drawbacks, including low resolution, the need to manipulate radioactive compounds, as well as the low availability of PET scanners for routine diagnostic purposes in patients suffering from neurodegenerative diseases and of μPET devices for preclinical studies in animals. Thus, alternative methods based on other imaging modalities, such as MRI, are currently being developed to detect amyloid plaques.

Compared to PET imaging, MRI has a higher resolution, does not require radioactive compounds, and MR spectrometers are more readily available than PET scanners. The imaging of amyloid plaques by MRI can be achieved by exploiting the spontaneous contrast of the plaques or by using NMR contrast agents. The detection of amyloid plaques on the basis of their spontaneous contrast mainly relies on the accumulation of iron in the core of these lesions which leads to hypointense spots on T2, T2* or susceptibility-weighted MR images in transgenic mice (Chamberlain et al., 2009; Dhenain et al., 2009; Jack et al., 2005) and *post-mortem* human brain samples (Meadowcroft et al., 2009). However, iron accumulation in amyloid plaques is not homogenously

* Corresponding author at: MIRCen, URA CEA CNRS 2210, 18 route du Panorama, 92 265, Fontenay-aux-Roses, Cedex, France. Fax: +33 1 46 54 84 51.
E-mail addresses: mathieu.santin@icm-institute.org (M.D. Santin), Thomas.Debeir@sanofi.com (T. Debeir), lori.bridal@upmc.fr (S.L. Bridal), thomas.rooney@sanofi.com (T. Rooney), Marc.Dhenain@cea.fr (M. Dhenain).
[1] Present address: Institut du Cerveau et de la Moelle épinière (ICM), Centre de NeuroImagerie de Recherche (CENIR) – Hôpital Pitié-Salpêtrière – 47/83 Boulevard de l'Hôpital – 75013 Paris, France.

1053-8119/$ – see front matter © 2013 Published by Elsevier Inc.
http://dx.doi.org/10.1016/j.neuroimage.2013.04.106

distributed in all brain regions (Dhenain et al., 2009) and the detection of amyloid plaques by using spontaneous contrast can be very challenging and time consuming (Dhenain et al., 2002). As a result approaches based on the use of targeted or non-targeted contrast agents are being used to improve the detection of amyloid plaques by MRI.

The most commonly used targeted contrast agents rely on the targeting of Aβ peptides or anti-amyloid antibodies that are linked to a contrastophore, such as Gadolinium (Gd) or monocrystalline iron oxide nanoparticules (MION) (Poduslo et al., 2002; Zaim Wadghiri et al., 2003). Methods, such as ICV-Gd-staining, which rely on intracerebro-ventricular (ICV) administration of a non-targeted contrast agent (*e.g.* Gadoteric acid (Dotarem®, Guerbet, France), can also be used to detect amyloid plaques in living mice with a very good resolution (45 μm) (Dhenain et al., 2006; Petiet et al., 2012). The underlying mechanisms of contrast enhancement are due to the hydrophilic properties of Gd that prevent it from associating with the highly hydrophobic amyloid plaques (Petiet et al., 2012). The ICV-Gd-staining protocol uses a commercially available and inexpensive contrast agent (Dotarem®), which is also an advantage compared to other methods. This agent does not interfere with amyloidogenesis, unlike specific contrast agents composed of Aβ fragments (Zaim Wadghiri et al., 2003) or Aβ antibodies (Poduslo et al., 2002), that are less suitable for longitudinal follow-up studies and the assessment of pharmacological treatments.

Since neither targeted nor non-targeted contrast agents readily cross the blood–brain barrier (BBB), the ability to detect amyloid plaques with these agents requires the use of specialized techniques to penetrate the BBB and deliver the contrast agent in the vicinity of the amyloid plaques. Examples of these techniques include, intracarotid arterial infusion of hyperosmolar solutions (Zaim Wadghiri et al., 2003), linkage of the contrast agents with polyamines, such as putrescine (Poduslo et al., 2002), liposomes or nanoparticle drug carriers (Gulyaev et al., 1999; Huwyler et al., 1996) and direct injection of the contrast agent into the brain ventricles. However, these techniques have only limited effects on drug uptake and can have toxic effects on brain tissues (Vykhodtseva et al., 2008). By contrast, the use of ultrasound (US) and gas microbubbles (also used as contrast agents in US imaging) is a very promising method to induce transient BBB opening which has been demonstrated to be selective, reversible and relatively non-invasive in mice (Choi et al., 2007; Hynynen et al., 2001; McDannold et al., 2005) and non-human primates (Marquet et al., 2011). In addition, several reports have shown that this technique is one of the least toxic methods that can be used to open the BBB and to enable the uptake of an agent into the brain (Howles et al., 2010a; Vykhodtseva et al., 2008).

The aim of the present study was to evaluate whether the use of unfocused US and microbubbles could be used to improve the ICV-Gd-staining protocol previously described by Petiet et al. (Petiet et al., 2012) by enabling the detection of amyloid plaques after intra-venous (IV) administration of a Gd contrast agent and thereby avoid the need for administration by ICV injection. Our data show that this new MR imaging method, called US–Gd-staining, can be used to rapidly detect amyloid plaques in the brain of transgenic mice.

Materials and methods

Animals

Experiments were conducted on female APP/PS1 transgenic mice overexpressing amyloid precursor protein (APP) and presenilin 1 (PS1) mutations associated with familial AD (double Thy1 APP751 SL Swedish (KM670/671NL) and London (V717I) mutations introduced in the human APP751 sequence × HMG PS1 M146L transgenic mouse line) (Blanchard et al., 2003; Delatour et al., 2006). In these animals, amyloid deposition starts at the age of 2.5 months (Blanchard et al., 2003). Amyloid-free PS1 mice were used as controls. A total of 12 animals aged from 8 to 17 month-old were used for this study (6 APP/PS1 and 6 PS1 controls). Animal experimental procedures were performed in strict accordance with the recommendations of the EEC (86/609/EEC) and the French national committee (decree 87/848) for the care and use of laboratory animals. The research was conducted under the authorization number 91-326 from the "Direction Départementale des Services Vétérinaires de l'Essonne".

In vivo MRI experiments

In vivo MRI was performed on a 7 T-Spectrometer (Agilent, USA) interfaced with a console running VnmrJ 2.3. The spectrometer was equipped with a rodent gradient insert of 700 mT/m. A birdcage coil (RapidBiomed, GmbH, Germany) and a mouse brain surface coil (RapidBiomed GmbH, Germany) were used for emission and reception, respectively. MR images were recorded using two different imaging sequences. First, a low resolution 3D-Gradient Echo sequence was used to monitor the efficiency of BBB opening (FOV = $20 \times 20 \times 13 mm^3$, Mtx = $128 * 128 * 64$, TR = 25 ms, TE = 2 ms, flip angle = 30°, Nex = 1, bandwidth = 100 kHz, acquisition time: 3 min 24 s (Howles et al., 2010a)). Second, a high-resolution 3D-Gradient Echo sequence was used to achieve a resolution of $29 * 29 * 117 \mu m^3$ allowing amyloid plaque imaging (FOV: $15 * 15 * 15 mm^3$, Mtx = $512 * 512 * 128$, TR = 30 ms, TE = 15 ms, flip angle = 20°, Nex = 1, bandwidth = 25 kHz, acquisition time: 32 min (Petiet et al., 2012)). All procedures requiring IV injection were performed after insertion of a catheter (27G, Microflex, Vygon, France) into the tail vein of the animals. The animals were imaged using different experimental protocols (Table 1): 1) IV administration of Gd contrast agent (Gd-DOTA, Dotarem®, Guerbet, France, 4 mmol/kg) after BBB opening with US and microbubbles, *i.e.* US–Gd-staining and 2) ICV administration of Gd contrast agent *i.e.* ICV-Gd-staining which is our previously established reference method to detect amyloid plaques by MRI (Petiet et al., 2012) and 3) four control conditions based on 3.1) no administration of Gd contrast agents or microbubbles and no stimulation by US (Ctrl), 3.2) no administration of Gd contrast agents and US stimulation of microbubbles (Ctrl-US-Bb), 3.3) IV administration of Gd contrast agent without stimulation by US and microbubbles (Ctrl-IVGd), 3.4) IV administration of Gd contrast agent with US stimulation but without microbubbles injection (Ctrl-IVGd-US). For all protocols, the MR images were recorded starting at 60 min after administration of the Gd-based contrast agent or US stimulation for the Ctrl-US-Bb condition. During the MRI experiment the animals were anesthetized with a mixture of isoflurane (0.75–1.5%) and carbogen (95% O2–5% CO2) and their breathing rate was monitored. Carbogen was used to reduce the signal coming from circulating blood (Thomas et al., 2003).

T1 was also evaluated to assess the dynamics of the Gd-based contrast agent wash-out after its penetration in the brain using BBB opening by ultrasound and microbubbles. The T1 calculation was based on seven successive 2D multi-slice spin echo images with five TR values (TR = 0.4, 0.75, 1.5, 2.5, and 5 s, TE = 14 ms, Nex = 1, FOV = $25 \times 25 mm^2$, Mtx = 128×128, 6 slices, slice thickness = 1 mm, bandwidth = 50 kHz). The images were recorded before US–Gd-staining and every 80 min over 8 h after the BBB opening. Parametric maps of relaxation times were calculated from exponential regression curves ($S = 1 - \exp(-TR / T1)$) where S is the

Table 1
Overview of the various protocols used in the current experiments.

	Administration of Gd contrast agent	Use of US stimulation	IV administration of microbubbles
US–Gd-stain	IV	Yes	Yes
ICV-Gd-stain	ICV	No	No
Ctrl	No	No	No
Ctrl-US–Bb	No	Yes	Yes
Ctrl-IVGd	IV	No	No
Ctrl-IVGd–US	IV	Yes	No

signal intensity, TR is the repetition time and T1 is the longitudinal relaxation time (ImageJ, MRI Analysis Calculator, Karl Schmidt). Relaxation times were measured from cortical regions in the frontal part of the brain.

BBB opening by ultrasound and microbubbles for US–Gd-staining

Ultrasound system

A single element unfocused transducer (center frequency: 1 MHz, diameter: 13 mm, Imasonic, France) was used throughout the study. Prior to experiments, the transducer field was characterized in a water tank filled with 4 L of deionized and degassed water. The transducer could be positioned along 3 orthogonal axes using a motion controller (MM4006, Newport, USA). The transducer was excited in pulse-echo mode using a pulser-receiver (5900PR, Olympus NDT Inc., USA). Signals reflected by a point-like reflector were amplified by the receiver and digitized using an oscilloscope (Tektronix TDS 1012, USA). Acquisition and transducer scanning were driven by in-house Matlab software (Mathworks, USA). To measure the −6 dB beam diameter (BD[−6 dB]) and near field distance (NF), ten 2D-scans were recorded with axial distances from 20 to 40 mm between the transducer and the point-like reflector. Fig. 1 shows the beam pattern measured based on maximum peak-to-peak voltage (maximum scaled to 0 dB) at each point in the 2D-scan at the near field distance (29.5 mm between the transducer and the point-like reflector). Near field distance is determined by the last maximum peak-to-peak voltage measured along the central axis of each 2D-scan. The theoretical (BD[−6 dB] ≈ 3.3 mm, NF ≈ 28.5 mm) and measured values (BD[−6 dB] ≈ 4.0 mm, NF ≈ 29.5 mm) of beam diameter and near field distances ($D^2/4\lambda$ with D the element diameter and λ the wavelength of the US wave in water) were in good agreement.

The transducer-induced pressure at the near field distance was then measured with a calibrated hydrophone (HGL-0400, Onda Corp, USA) in deionized and degassed water. An arbitrary function generator (G5100A, Picotest, Taiwan) and a 50-dB power amplifier (A075, Electronics and Innovation, USA) were used to generate sinusoidal tone bursts consisting of a 1-MHz centered burst of 10 000 cycles leading to a 10 ms excitation with a pulse repetition frequency (PRF) of 10 Hz. The peak-to-peak voltage (Vpp) given by the function generator varied linearly from 0.05 to 0.60 Vpp. The resulting peak negative acoustic pressures measured with the hydrophone ranged from 0.17 MPa to 1.70 MPa.

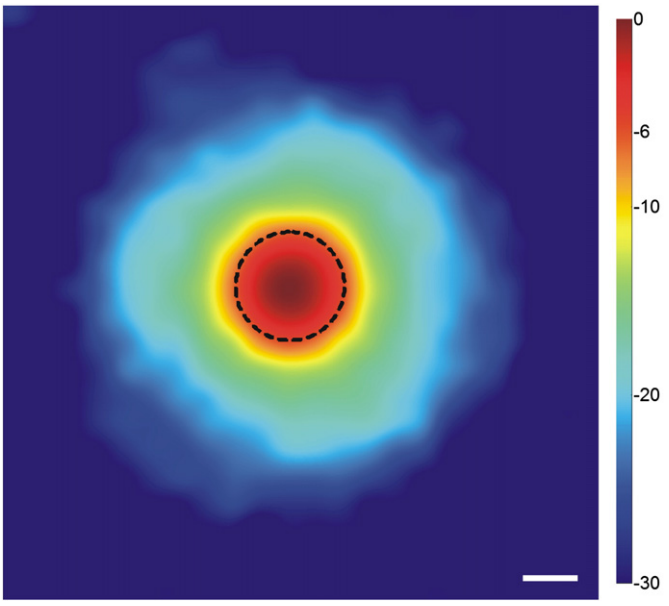

Fig. 1. Color-coded US beam pattern measured at the near field distance in dB. The black-dashed circle delimits the −6 dB zone (4 mm diameter). Scale bar = 2 mm.

BBB opening by ultrasound and microbubbles

Animals were anesthetized with a mixture of isoflurane (1–2%) and air (1 L/min) during the procedure of BBB opening by US and microbubbles. Their heads were shaved and placed in a supine position on top of a tank filled with 2 L of pure and degassed water. The transducer was placed in this tank beneath the head of the animals. The distance between the transducer membrane and the top of the head was adjusted to ensure that the near field distance of the transducer was within the mouse brain parenchyma. US excitation consisted of sinusoidal tone bursts with the same parameters and electronics used for the characterization of the transducer-induced pressure. The function generator peak-to-peak voltage was set to 0.40 Vpp to give a peak negative pressure of 1.1 MPa at the near field distance in water. This value was chosen on the basis of values reported in the literature to induce a transient BBB opening with a mechanical index (MI) above 0.5 (McDannold et al., 2008) and took into account US attenuation due to the skull (30% at 1.5 MHz (Choi et al., 2007)). US excitation lasted for 3 min. Two IV boluses of microbubbles (0.1 mL each; Sonovue®, Bracco Research SA, Switzerland) were administered at the beginning and 1 min after the start of US excitation. When used, the MR contrast agent was administered 10 and 11 min after the end of the US excitation (two boluses of 0.1 mL).

Surgical procedure for ICV-Gd-staining

To compare results between the US-based BBB opening method and direct injection into the brain ventricles, we performed ICV injections of MRI contrast agent in mice, as previously described (Petiet et al., 2012). Briefly, the mice were anesthetized with a mixture of isoflurane (1–2%) and air (1 L/min). They were placed on a stereotaxic frame and the skull was bilaterally perforated with a Dremel. Blunt Hamilton syringes were used to inject MR contrast agent into the lateral ventricles at coordinates A/P −0.2 mm, L ± 1 mm, −1.8 mm relative to the surface of the dura mater (Paxinos and Franklin, 2001). A volume of 1 μL (0.5 mmol/mL) was injected into each side at a rate of 0.2 μL/min. Upon completion of the injections, the needles were slowly withdrawn to minimize any outflow from pressure release and the skin was then sutured.

Amyloid load quantification from MR images

Cortical amyloid load was calculated from MR images of animals that underwent US–Gd-staining procedure by using a method similar to that previously reported procedure (Jack et al., 2005; Petiet et al., 2012). Briefly, 8 coronal slices (antero-posterior direction), evenly spaced by 468 μm, were selected and 4 circular ROIs (surface ~1 mm^2 each) were drawn on each of these slices (2 in each hemisphere). The 8 slices were positioned so that the third slice was localized at the level of the anterior commissure. Hypointense spots were manually counted, excluding hypointense elements that could be followed over more than 2 adjacent slices, or that had a tube-like shape, suggesting the presence of a blood vessel. Areas of hypointense spots were measured in each ROI. Plaque load was determined as the ratio of the mean area of the hypointense spots multiplied by the number of spots counted over the area of the ROI.

Histology — correlation with in vivo MRI

All animals were sacrificed after the MRI exams using a high dose of sodium pentobarbital (100 mg/kg) and then perfusion-fixed with 10% buffered formalin. Their brains were then removed, immersed in formalin for at least 24 h and stored at 4 °C. The brains of the animals were cryoprotected in sucrose (15% for 24 h then 30% for 24 h) and cut into

40-μm thick coronal sections on a freezing microtome. The sections were stained for β-amyloid deposits (anti-β-amyloid immunohistochemistry) to detect amyloid plaques. The sections were first rinsed in phosphate buffered saline (PBS 0.1 M) and then in 30% hydrogen peroxide. They were then pretreated with 0.2% octylphenol ethylene oxide condensate (Triton X-100™, Sigma). After this pretreatment, they were incubated with an anti-amyloid primary antibody (monoclonal BAM10 clone A3981, dilution 1:1000, Sigma-Aldrich®) for 48 h and then with a secondary antibody (biotinated IgG anti-mouse, BA-9200, dilution 1:1000, Vector® Laboratories, Burlingame, USA) for 1 h. Before revelation (VIP substrate kit for peroxidase, Vector® Labs) the reaction was amplified for 1 h with a biotin-avidin complex (ABC Vectastain kit, Vector® Labs) (Berghorn et al., 1994). All sections were digitized using a microscope (Axioplan-1TM, Zeiss Inc.) connected to a digital camera (MicrofireTM, Optronics Inc.). Three-dimensional MR images were manually registered to histological sections using the "3D/Volume viewer" plugin from ImageJ (Rasband, 1997–2012). This plugin enables manual rotation of the 3D MR images in any direction. We focused on histological sections at the level of the hippocampus and identified typical landmarks such as the layers of the hippocampus, blood vessels or amyloid plaques. The 3D MRI images were then manually rotated until we could identify these landmarks in the MR images.

Results

In vivo MRI after opening of the BBB by US and microbubbles

Low resolution MR images were first recorded to evaluate BBB opening in control mice. Visual inspection of images recorded in the first control conditions, *i.e.* no injection of Gd-based contrast agent without (Ctrl condition, Fig. 2A) or with (Ctrl–US–Bb condition, Fig. 2B) administration of microbubbles and US revealed images with a poor contrast and low signal to noise ratio. The second control condition based on administration of Gd-based contrast agent either without US stimulation (Ctrl-IVGd condition, Fig. 2C) or with US stimulation in the absence of microbubbles (Ctrl-IVGd–US condition, Fig. 2D) induced a signal increase mainly within the cerebral ventricles, muscles and peripheral fat. The administration of Gd-based contrast agent with US stimulation and injection of microbubbles induced an increased signal in the cerebral ventricles and cerebral parenchyma, as well as in the tissues surrounding the brain (US–Gd-staining condition, Fig. 2E). The signal increase in the brain was similar to that obtained after ICV injection of the contrast agent (ICV-Gd-staining condition, Fig. 2F). Measures of relaxation times showed that the cortical T1 dropped from 2000 ms to ~360 ms 80 min post US–Gd-staining (Fig. 2G). The T1 progressively returned to its initial value ~8 h (480 min) after the BBB opening. This suggests that the contrast agent was cleared out of the cortex at that time.

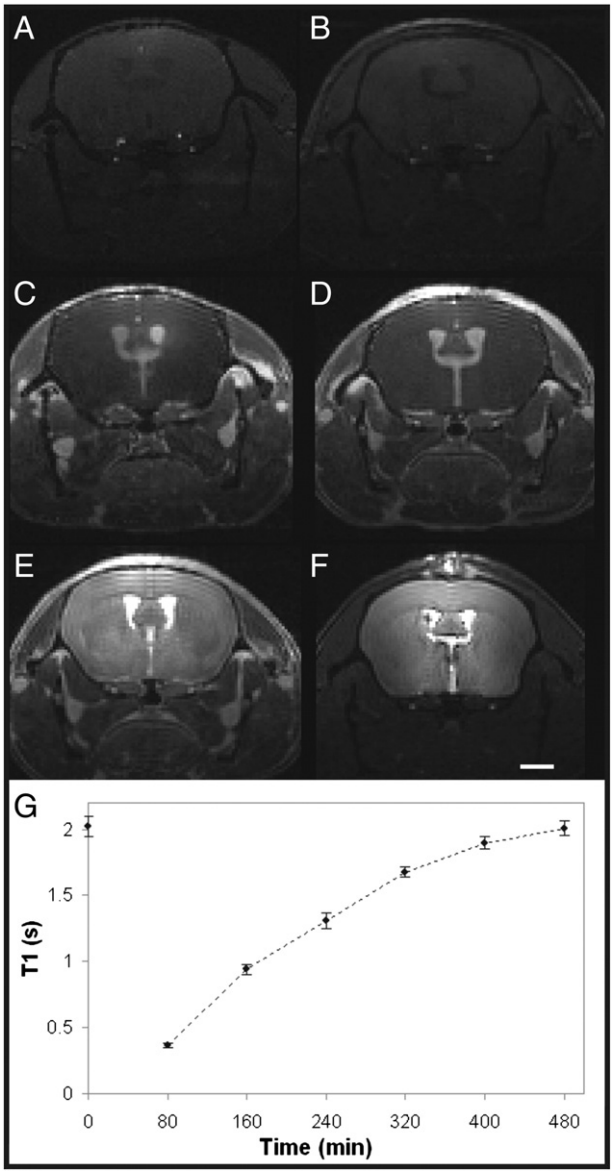

Fig. 2. Low resolution MR images of brains from mice that were not injected with Gd contrast agent and did not receive microbubbles/US stimulation (A — Ctrl condition), that were not injected with Gd contrast agent but received microbubbles/US stimulation (B — Ctrl-US–Bb condition), that were injected with contrast agent alone (C — Ctrl-IVGd condition), that were injected with contrast agent and received US stimulation without microbubbles (D — Ctrl-IVGd–US condition), that were injected with contrast agent and received microbubbles/US stimulation (E — US–Gd-staining condition), and after ICV injection of Gd-based contrast agent (F — ICV-Gd-staining condition). G. Longitudinal follow-up of T1 signal recovery after administration of contrast agent and microbubbles/US stimulation. Scale bar = 2 mm.

In vivo MRI detection of amyloid plaques after US–Gd-staining

High resolution images ($29 \times 29 \times 117 \mu m^3$, acquisition time: 32 min) of the brains of APP/PS1 mice and control amyloid-free PS1 mice were recorded after US–Gd-staining, ICV-Gd-staining and in control conditions. In APP/PS1 mice, hypointense spots were detected in the cerebral cortex after US–Gd-staining (Figs. 3A–B,4A). Similar spots were detected after ICV-Gd-staining (Figs. 3C–D), a method previously shown to detect amyloid plaques (Petiet et al., 2012). Cerebral images of APP/PS1 mice recorded without IV injection of Gd and after IV injection of microbubbles and US stimulation (Ctrl-US-Bb condition, Fig. 3E) or without US stimulation (Ctrl condition, data not shown) had a poor signal to noise ratio and did not display any hypointense spots. IV injection of Gd-based contrast agent alone produced a signal enhancement in the cerebral ventricles, but a low signal increase in the cerebral parenchyma (Ctrl-IVGd condition, Fig. 3F). Amyloid plaques could not be detected in either of these images. A similar result was obtained after IV administration of Gd-based contrast agent and US stimulation in the absence of microbubbles injection (Ctrl-IVGd–US condition, data not shown). Images of the brains of control amyloid-free PS1 mice recorded after US–Gd-staining (Figs. 3G and 4C) had a signal enhancement in the parenchyma but did not display any hypointense spots. Hypointense spots observed on the MR images recorded after US–Gd-staining were colocalized with amyloid plaques detected on histological sections (Figs. 4A–B (arrows)) thereby confirming that the hypointense spots detected with US–Gd-staining are amyloid plaques. We were also able to detect an increase in amyloid load between 8 month old mice (5.1 ± 1.0%) and 17 month old mice (9.1 ± 2.8%). In addition, two 8 month-old APP/PS1 were imaged twice and the amyloid load quantified was found to be very reproducible (5.1 and 5.3% for

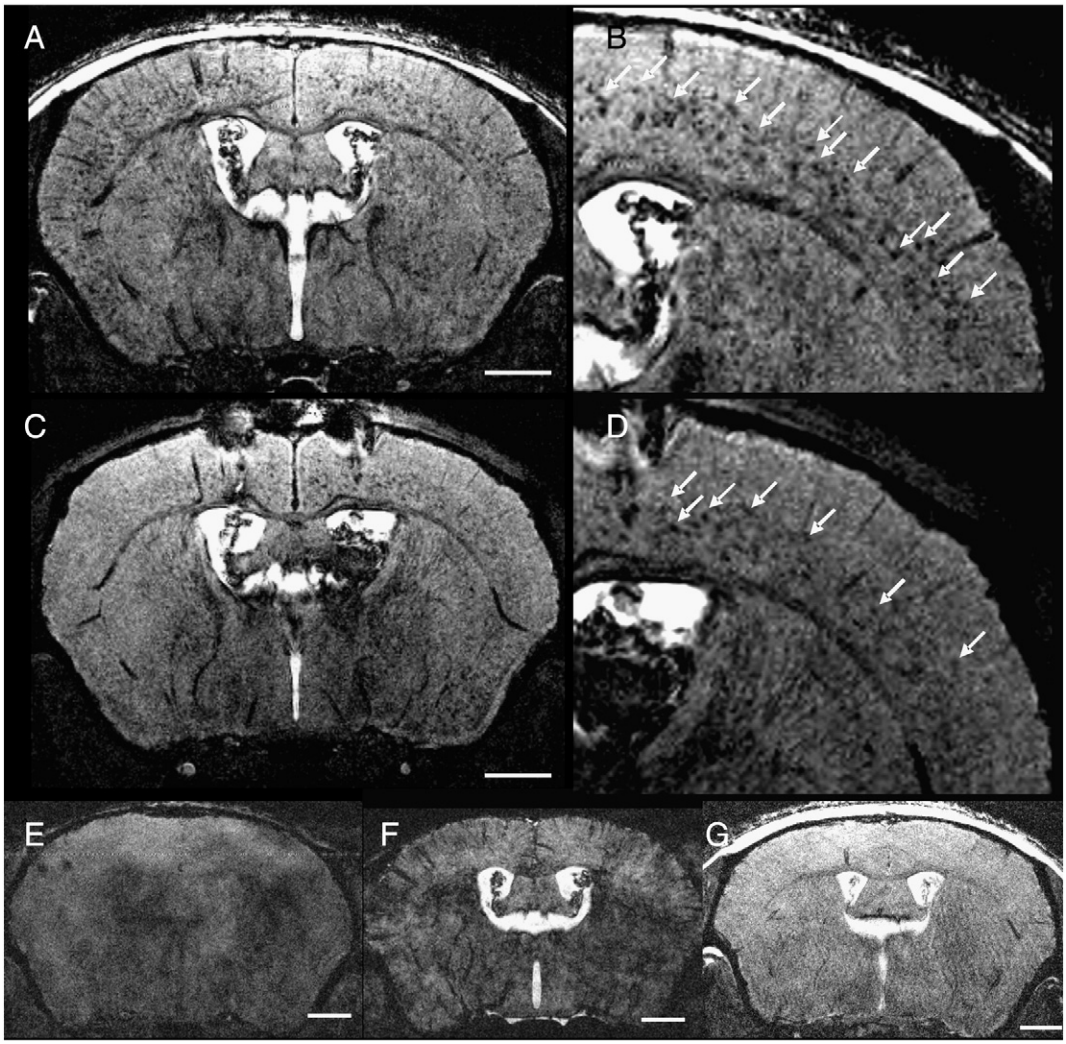

Fig. 3. High resolution MR images (29 × 29 × 117μm3) of the brains of APP/PS1 mice and control amyloid-free PS1 mice and comparison with histological detection of amyloid plaques. Hypointense spots (arrows) detected in the cerebral cortex of APP/PS1 mice after US–Gd-staining (A and B) or ICV-Gd-staining (C and D). Cerebral MR images of an APP/PS1 mouse that was not injected with Gd contrast agent but received microbubbles/US stimulation (E — Ctrl-US–Bb condition), that was injected with Gd contrast agent alone and showed signal enhancement in the cerebral ventricles (F — Ctrl-IVGd condition). (G) Signal enhancement in the parenchyma, but no detection of hypointense spots, in the brain of a control amyloid-free PS1 mouse after US–Gd-staining. Scale bars = 2 mm.

the first mouse and 7.3 and 7.7% for the second one) using a test/re-test protocol.

Discussion

In the present study we have described a novel method that enables the MRI imaging of amyloid plaques in the brain of transgenic mice after the IV injection of a non-targeted MRI contrast agent that is approved for clinical use in humans. The protocol used also allows the detection of amyloid plaques by using a very short imaging time (32 min) and a very high in-plane resolution (29 μm). We focused on amyloid plaques present in the cortex and hippocampus as these are the regions that are typically affected in AD. Plaques from the subcortical regions, such as the striatum, could also be detected but are

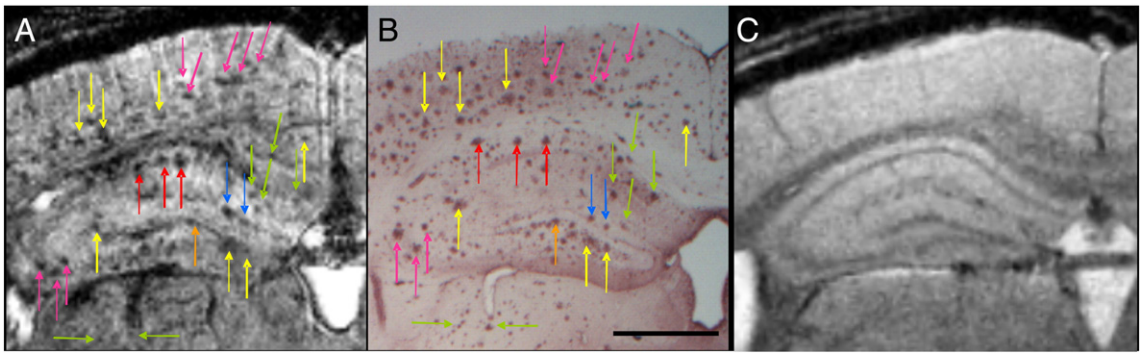

Fig. 4. Hypointense spots seen on MR images recorded after US–Gd-staining (A) were colocalized with amyloid plaques detected on histological sections (B) (arrows). (C) Shows the MR image of a control mouse after US–Gd-staining. Hypointense spots were not visible on this image. Scale bar = 1 mm.

more difficult to dissociate from white matter bundles that also appear as hypointense spots after Gd-staining.

The imaging of amyloid plaques by MRI in humans and animals has been widely studied and several protocols based on the natural contrast of amyloid plaques (Braakman et al., 2006; Jack et al., 2005) or using targeted and non-targeted contrast agents have been reported (Petiet et al., 2012; Poduslo et al., 2002; Zaim Wadghiri et al., 2003). To the best of our knowledge, the previous *in vivo* MRI studies that detected amyloid plaques without using Gd-staining protocols were recorded with an in plane resolution lower than 60 μm before zero-filling (Braakman et al., 2006; Jack et al., 2005; Sigurdsson et al., 2008) and with imaging time longer than 90 min (except in the study by Braakman et al., 2006). Our protocol enables a shorter imaging time and an increased resolution due to the high cerebral signal induced by the penetration of the contrast agent in the brain parenchyma. The Gd-based contrast agent is cleared out of the brain within approximately 8 h after administration by US–Gd-staining which is consistent with previous studies by ICV-Gd-staining where clearance of the Gd-based contrast agent occurred between 4.5 and 24 h (Petiet et al., 2012).

We have previously shown that the ICV-Gd-staining method can detect age-dependent increases of amyloid plaque load (Petiet et al., 2012). Here we confirm that an age-dependent increase of amyloid load can also be detected with the US–Gd-staining method and that this method has consistent test/re-test sensitivity. Moreover, the amyloid load detected in the APP/PS1 mice with US–Gd-staining is similar to that previously reported with ICV-Gd-staining ($5.5 \pm 0.9\%$ and $5.1 \pm 1.0\%$ at 8 months and $9.7\% \pm 2.3\%$ and $9.1 \pm 2.8\%$ at 17.5 and 17 months for ICV-Gd-staining and US–Gd-staining, respectively (Petiet et al., 2012)). In this previous study, we also showed a good correlation between amyloid load quantified by MRI and histology, which suggests that Gd-staining methods can be used to provide quantitative markers to study anti-amyloid therapies. Our data also demonstrate that repeated opening of the BBB is feasible without toxic side effects, since we were able to use the US–Gd-staining protocol to image each mouse on at least two occasions. However, further studies are necessary to evaluate the potential long term side effects of the US–Gd-staining protocol.

In previous studies using contrast agents to detect amyloid plaques, the contrast agents did not readily cross the BBB and needed to be administered in combination with agents, such as mannitol or putrescine to open the BBB (Poduslo et al., 2002; Zaim Wadghiri et al., 2003) or required ICV injection (Petiet et al., 2012). With ICV injection the contrast agent had to diffuse from the ventricle to the whole brain which can lead to a low signal enhancement in regions far from the injection sites and impeded amyloid plaque detection in these regions. Moreover, ICV injections are susceptible to induce imaging artefacts close to the site of the surgery. The novel method described here combines two previously published procedures and is based on the ability of non-targeted Gd-based MR contrast agents to detect amyloid plaques when administered in the brain (Petiet et al., 2012) and the ability to transiently open the BBB using US and microbubbles to enable drug delivery in the brain of rodents and non-human primates (Marquet et al., 2011; O'Reilly and Hynynen, 2012; Treat et al., 2012). This technique has also been used to administer MR contrast agents such as Manganese Chloride into the brain and to perform Manganese-enhanced MRI (MEMRI) functional imaging (Howles et al., 2010b).

The opening of the BBB after administration of US and microbubbles can be obtained by using focused (Hynynen, 2008) or unfocused US (Howles et al., 2010b). Focused US opens the BBB very locally and is used to target precise anatomical regions *e.g.* to deliver genes or focused therapies (Hynynen, 2008; Jordao et al., 2011) whereas unfocused US opens the BBB over a larger area of the brain which explains its use to deliver contrast agents that have to reach the whole brain (Howles et al., 2010a). We chose to use unfocused US since a large penetration of the Gd contrast agent was required to homogeneously label the amyloid plaques. Moreover, the method has been shown to be safe and does not induce any behavioral alterations in mice (Howles et al., 2010a) and BBB opening by using ultrasound stimulation without microbubbles can be performed without producing any lesion (Ballantine et al., 1960). However more recent studies have shown that administration of microbubbles in conjunction with US stimulation reduces the acoustic energy needed to produce the BBB opening (Vykhodtseva et al., 1995) and limits the interaction of the ultrasound with the endothelial cells thereby reducing the chance of damage to other brain structures (Vykhodtseva et al., 2008). This justifies the use of US and microbubbles in the current protocol.

The opening of the BBB with US and microbubbles can be modulated by varying different parameters, including the pulse repetition frequency (PRF), the duration of excitation bursts and the number of cycles of the acoustic excitation. Variations of many of these parameters have already been investigated for focused US (Choi et al., 2011; O'Reilly et al., 2011) but it is difficult to extrapolate the results from these studies to unfocused US protocols. Furthermore, refinement of the unfocused US–Gd-staining protocol will require the evaluation of the effects of modulating these parameters on US–Gd-staining efficacy. For example, the quality of the BBB disruption is expected to be linked to the amount of fresh microbubbles brought by the bloodstream below the ultrasound beam before an excitation burst. The amount of fresh microbubbles is modulated by the PRF which regulates the delay between two successive excitations and the effect of this parameter on the quality of BBB disruption is expected to be strong after unfocused US as the insonified volume (the beam size) is large as compared to focused US. We can therefore expect that short PRF leads to a reduced number of fresh microbubbles experiencing excitation between two cycles which could lead to a reduced opening of the BBB. By contrast, long PRF leads to an increased number of fresh bubbles experiencing excitation between two cycles which could lead to a better opening of the BBB.

In conclusion, we have developed a new experimental protocol to detect amyloid plaques in transgenic AD mice by MRI. This protocol has a short imaging time, a high in-plane resolution (29 μm) and uses an inexpensive contrast agent that can be obtained in any laboratory. It can be used repeatedly to follow the progression of AD in longitudinal studies in the same animal and has the potential to evaluate the activity of amyloid lowering therapeutic strategies on disease progression. This technique also has the potential to be used with other contrast agents, such as targeted agents. The opening of the BBB with US and microbubbles has been used in animal studies for more than 10 years and ongoing studies are being performed to implement this technique in humans. For example, commercial prototypes have been developed for clinical applications and have been successfully tested in large animals (Beccaria et al., in press; McDannold et al., 2012). These prototypes seem to be now ready for phase 1 studies to administer drugs locally in the brain of patients with brain cancer (Beccaria et al., in press). Although US and microbubbles cannot be currently used to open the BBB in humans, further development of this technology may enable a local opening of the BBB to evaluate amyloid load in the brain by MRI. Our study also provides a proof of concept for the use of US–Gd-staining to detect amyloid plaques by MR imaging after peripheral injection of a non-targeted contrast agent.

Acknowledgments

Our work was supported by Medicen (Pôle de compétitivité Île-de-France, TransAl program), the France-Alzheimer association, the France-Berkeley fund, and the NIH R01-AG020197. We thank F. Petit and C. Jan from CEA MIRCen for participation in the histological studies.

Conflict of interest statement

The authors declare that there are no conflicts of interest.

References

Ballantine Jr., H.T., Bell, E., Manlapaz, J., 1960. Progress and problems in the neurological applications of focused ultrasound. J. Neurosurg. 17, 858–876.

Beccaria, K., Canney, M., Goldwirt, L., Fernandez, C., Adam, C., Piquet, J., Autret, G., Clement, O., Lafon, C., Chapelon, J.-Y., Carpentier, A., 2013. Opening of the blood–brain barrier with an unfocused ultrasound device in rabbits. J. Neurosurg. (in press).

Berghorn, K.A., Bonnett, J.H., Hoffman, G.E., 1994. cFos immunoreactivity is enhanced with biotin amplification. J. Histochem. Cytochem. 42, 1635–1642.

Blanchard, V., Moussaoui, S., Czech, C., Touchet, N., Bonici, B., Planche, M., Canton, T., Jedidi, I., Gohin, M., Wirths, O., Bayer, T.A., Langui, D., Duyckaerts, C., Tremp, G., Pradier, L., 2003. Time sequence of maturation of dystrophic neurites associated with Ab deposits in APP/PS1 transgenic mice. Exp. Neurol. 184, 247–263.

Braakman, N., Matysik, J., van Duinen, S.G., Verbeek, F., Schliebs, R., de Groot, H.J., Alia, A., 2006. Longitudinal assessment of Alzheimer's beta-amyloid plaque development in transgenic mice monitored by *in vivo* magnetic resonance microimaging. J. Magn. Reson. Imaging 530–536.

Chamberlain, R., Reyes, D., Curran, G.L., Marjanska, M., Wengenack, T.M., Poduslo, J.F., Garwood, M., Jack Jr., C.R., 2009. Comparison of amyloid plaque contrast generated by T2-weighted, T2*-weighted, and susceptibility-weighted imaging methods in transgenic mouse models of Alzheimer's disease. Magn. Reson. Med. 61, 1158–1164.

Choi, J.J., Pernot, M., Small, S.A., Konofagou, E.E., 2007. Noninvasive, transcranial and localized opening of the blood–brain barrier using focused ultrasound in mice. Ultrasound Med. Biol. 33, 95–104.

Choi, J.J., Selert, K., Gao, Z., Samiotaki, G., Baseri, B., Konofagou, E.E., 2011. Noninvasive and localized blood–brain barrier disruption using focused ultrasound can be achieved at short pulse lengths and low pulse repetition frequencies. J. Cereb. Blood Flow Metab. 31, 725–737.

Delatour, B., Guegan, M., Volk, A., Dhenain, M., 2006. *In vivo* MRI and histological evaluation of brain atrophy in APP/PS1 transgenic mice. Neurobiol. Aging 27, 835–847.

Dhenain, M., Privat, N., Duyckaerts, C., Jacobs, R.E., 2002. Senile plaques do not induce susceptibility effects in T2*-weighted MR microscopic images. NMR Biomed. 15, 197–203.

Dhenain, M., Delatour, B., Walczak, C., Volk, A., 2006. Passive staining: a novel *ex vivo* MRI protocol to detect amyloid deposits in mouse models of Alzheimer's disease. Magn. Reson. Med. 55, 687–693.

Dhenain, M., El Tannir El Tayara, N., Wu, T.-D., Guegand, M., Volk, A., Quintana, C., Delatour, B., 2009. Characterization of *in vivo* MRI detectable thalamic amyloid plaques from APP/PS1 mice. Neurobiol. Aging 30, 41–53.

Doraiswamy, P.M., Sperling, R.A., Coleman, R.E., Johnson, K.A., Reiman, E.M., Davis, M.D., Grundman, M., Sabbagh, M.N., Sadowsky, C.H., Fleisher, A.S., Carpenter, A., Clark, C.M., Joshi, A.D., Mintun, M.A., Skovronsky, D.M., Pontecorvo, M.J., 2012. Amyloid-beta assessed by florbetapir F 18 PET and 18-month cognitive decline: a multicenter study. Neurology 79, 1636–1644.

Gulyaev, A.E., Gelperina, S.E., Skidan, I.N., Antropov, A.S., Kivman, G.Y., Kreuter, J., 1999. Significant transport of doxorubicin into the brain with polysorbate 80-coated nanoparticles. Pharmacol. Res. 16, 1564–1569.

Hardy, J., Selkoe, D.J., 2002. The amyloid hypothesis of Alzheimer's disease: progress and problems on the road to therapeutics. Science 297, 353–356.

Howles, G.P., Bing, K.F., Qi, Y., Rosenzweig, S.J., Nightingale, K.R., Johnson, G.A., 2010. Contrast-enhanced *in vivo* magnetic resonance microscopy of the mouse brain enabled by noninvasive opening of the blood–brain barrier with ultrasound. Magn. Reson. Med. 64, 995–1004.

Howles, G.P., Qi, Y., Johnson, G.A., 2010. Ultrasonic disruption of the blood–brain barrier enables *in vivo* functional mapping of the mouse barrel field cortex with manganese-enhanced MRI. NeuroImage 50, 1464–1471.

Huwyler, J., Wu, D., Pardridge, W.M., 1996. Brain drug delivery of small molecules using immunoliposomes. Proc. Natl. Acad. Sci. U. S. A. 93, 14164–14169.

Hynynen, K., 2008. Ultrasound for drug and gene delivery to the brain. Adv. Drug Deliv. Rev. 60, 1209–1217.

Hynynen, K., McDannold, N., Vykhodtseva, N., Jolesz, F.A., 2001. Noninvasive MR imaging-guided focal opening of the blood–brain barrier in rabbits. Radiology 220, 640–646.

Jack Jr., C.R., Wengenack, T.M., Reyes, D.A., Garwood, M., Curran, G.L., Borowski, B.J., Lin, J., Preboske, G.M., Holasek, S.S., Adriany, G., Poduslo, J.F., 2005. *In vivo* magnetic resonance microimaging of individual amyloid plaques in Alzheimer's transgenic mice. J. Neurosci. 25, 10041–10048.

Jordao, J.F., Ayala-Grosso, C.A., Markham, K., Huang, Y., Chopra, R., McLaurin, J., Hynynen, K., Aubert, I., 2011. Antibodies targeted to the brain with image-guided focused ultrasound reduces amyloid-beta plaque load in the TgCRND8 mouse model of Alzheimer's disease. PLoS One 5, e10549.

Klunk, W.E., Engler, H., Nordberg, A., Wang, Y., Blomqvist, G., Holt, D.P., Bergstrom, M., Savitcheva, I., Huang, G.F., Estrada, S., Ausen, B., Debnath, M.L., Barletta, J., Price, J.C., Sandell, J., Lopresti, B.J., Wall, A., Koivisto, P., Antoni, G., Mathis, C.A., Langstrom, B., 2004. Imaging brain amyloid in Alzheimer's disease with Pittsburgh Compound-B. Ann. Neurol. 55, 306–319.

Klunk, W.E., Lopresti, B.J., Ikonomovic, M.D., Lefterov, I.M., Koldamova, R.P., Abrahamson, E.E., Debnath, M.L., Holt, D.P., Huang, G.F., Shao, L., DeKosky, S.T., Price, J.C., Mathis, C.A., 2005. Binding of the positron emission tomography tracer Pittsburgh compound-B reflects the amount of amyloid-beta in Alzheimer's disease brain but not in transgenic mouse brain. J. Neurosci. 25, 10598–10606.

Maeda, J., Zhang, M.R., Okauchi, T., Ji, B., Ono, M., Hattori, S., Kumata, K., Iwata, N., Saido, T.C., Trojanowski, J.Q., Lee, V.M., Staufenbiel, M., Tomiyama, T., Mori, H., Fukumura, T., Suhara, T., Higuchi, M., 2011. *In vivo* positron emission tomographic imaging of glial responses to amyloid-beta and tau pathologies in mouse models of Alzheimer's disease and related disorders. J. Neurosci. 31, 4720–4730.

Mangialasche, F., Solomon, A., Winblad, B., Mecocci, P., Kivipelto, M., 2010. Alzheimer's disease: clinical trials and drug development. Lancet Neurol. 9, 702–716.

Marquet, F., Tung, Y.S., Teichert, T., Ferrera, V.P., Konofagou, E.E., 2011. Noninvasive, transient and selective blood–brain barrier opening in non-human primates *in vivo*. PLoS One 6, e22598.

McDannold, N., Vykhodtseva, N., Raymond, S., Jolesz, F.A., Hynynen, K., 2005. MRI-guided targeted blood–brain barrier disruption with focused ultrasound: histological findings in rabbits. Ultrasound Med. Biol. 31, 1527–1537.

McDannold, N., Vykhodtseva, N., Hynynen, K., 2008. Effects of acoustic parameters and ultrasound contrast agent dose on focused-ultrasound induced blood–brain barrier disruption. Ultrasound Med. Biol. 34, 930–937.

McDannold, N., Arvanitis, C.D., Vykhodtseva, N., Livingstone, M.S., 2012. Temporary disruption of the blood–brain barrier by use of ultrasound and microbubbles: safety and efficacy evaluation in rhesus macaques. Cancer Res. 72, 3652–3663.

Meadowcroft, M.D., Connor, J.R., Smith, M.B., Yang, Q.X., 2009. MRI and histological analysis of beta-amyloid plaques in both human Alzheimer's disease and APP/PS1 transgenic mice. J. Magn. Reson. Imaging 29, 997–1007.

O'Reilly, M.A., Hynynen, K., 2012. Ultrasound enhanced drug delivery to the brain and central nervous system. Int. J. Hyperthermia 28, 386–396.

O'Reilly, M.A., Waspe, A.C., Ganguly, M., Hynynen, K., 2011. Focused-ultrasound disruption of the blood–brain barrier using closely-timed short pulses: influence of sonication parameters and injection rate. Ultrasound Med. Biol. 37, 587–594.

Paxinos, G., Franklin, K.B.J., 2001. The Mouse Brain in Stereotaxic Coordinates, second ed. Academic Press, San Diego.

Petiet, A., Santin, M., Bertrand, A., Wiggins, C.J., Petit, F., Houitte, D., Hantraye, P., Benavides, J., Debeir, T., Rooney, T., Dhenain, M., 2012. Gadolinium-staining reveals amyloid plaques in the brain of Alzheimer's transgenic mice. Neurobiol. Aging 33, 1533–1544.

Poduslo, J.F., Wengenack, T.M., Curran, G.L., Wisniewski, T., Sigurdsson, E.M., Macura, S.I., Borowski, B.J., Jack Jr., C.R., 2002. Molecular targeting of Alzheimer's amyloid plaques for contrast-enhanced magnetic resonance imaging. Neurobiol. Dis. 11, 315–329.

Poisnel, G., Dhilly, M., Moustie, O., Delamare, J., Abbas, A., Guilloteau, D., Barre, L., 2012. PET imaging with [18F]AV-45 in an APP/PS1-21 murine model of amyloid plaque deposition. Neurobiol. Aging 33, 2561–2571.

Rasband, W.S., 1997-2012. ImageJ, U. S. http://imagej.nih.gov/ij/ National Institutes of Health, Bethesda, Maryland, USA.

Sigurdsson, E.M., Wadghiri, Y.Z., Mosconi, L., Blind, J.A., Knudsen, E., Asuni, A., Scholtzova, H., Tsui, W.H., Li, Y., Sadowski, M., Turnbull, D.H., de Leon, M.J., Wisniewski, T., 2008. A non-toxic ligand for voxel-based MRI analysis of plaques in AD transgenic mice. Neurobiol. Aging 29, 836–847.

Sperling, R.a, Aisen, P.S., Beckett, L.a, Bennett, D.a, Craft, S., Fagan, A.M., Iwatsubo, T., Jack, C.R., Kaye, J., Montine, T.J., Park, D.C., Reiman, E.M., Rowe, C.C., Siemers, E., Stern, Y., Yaffe, K., Carrillo, M.C., Thies, B., Morrison-Bogorad, M., Wagster, M.V., Phelps, C.H., 2011. Toward defining the preclinical stages of Alzheimer's disease: recommendations from the National Institute on Aging and the Alzheimer's Association workgroup. Alzheimers Dement. 7, 280–292.

Thomas, C., Chenu, E., Walczak, C., Plessis, M., Perin, F., Volk, A., 2003. Morphological and carbogen-based functional MRI of a chemically induced liver tumor model in mice. Magn. Reson. Med. 50, 522–530.

Treat, L.H., McDannold, N., Zhang, Y., Vykhodtseva, N., Hynynen, K., 2012. Improved anti-tumor effect of liposomal doxorubicin after targeted blood–brain barrier disruption by MRI-guided focused ultrasound in rat glioma. Ultrasound Med. Biol. 38, 1716–1725.

Vykhodtseva, N.I., Hynynen, K., Damianou, C., 1995. Histologic effects of high intensity pulsed ultrasound exposure with subharmonic emission in rabbit brain *in vivo*. Ultrasound Med. Biol. 21, 969–979.

Vykhodtseva, N., McDannold, N., Hynynen, K., 2008. Progress and problems in the application of focused ultrasound for blood–brain barrier disruption. Ultrasonics 48, 279–296.

Zaim Wadghiri, Y., Sigurdsson, E.M., Sadowski, M., Elliott, J.I., Li, Y., Scholtzova, H., Tang, C.Y., Aguilnaldo, G., Pappolla, M., Duff, K., Wisniewski, T.M., Turnbull, D.H., 2003. Detection of Alzheimer's amyloid in transgenic mice using magnetic resonance microimaging. Magn. Reson. Med. 50, 293–302.